Beni-Suef University Journal of Basic and Applied Sciences

RESEARCH

Open Access

Wear characteristics of laser-deposited AlCoCrCuFeNi high entropy alloy with finite element analysis

Modupeola Dada[1*], Patricia Popoola[1], Ntombi Mathe[2] and Samson Adeosun[3,4]

Abstract

Background: Wear is a destructive phenomenon and one of the principal causes of material failure in moving components during surface interaction while in service. AlCoCrCuFeNi high-entropy alloy with its many properties is a potential material for aero-engine applications attributed to its outstanding relatively lightweight, high strength, good thermal, oxidation, and corrosion resistance properties. Hence, the investigation into the tribological behaviour of AlCoCrCuFeNi high-entropy alloys is essential to reduce maintenance costs and prolong the service life of this advanced material for aerospace applications. Most AlCoCrCuFeNi high-entropy alloy compositions were fabricated via arc melting, which has been reported to have defects attributed to slow solidification, consequently reducing the mechanical properties of the alloy with limited reports on other fabrication methods. Therefore, there is a need for the use of advanced manufacturing techniques for fabricating these alloys to improve the tribological properties. In this study, AlCoCrCuFeNi high-entropy alloy was fabricated via laser metal deposition. The influence of the laser processing parameters, rapid solidification, and the applied load on the tribological properties of the as-built alloys under dry conditions has been studied for aerospace applications. The counter ball rolling friction analysis was also investigated using COMSOL Multiphysics.

Results: The results showed that at a high laser power of 1600 W and a scan speed of 12 mm/s, the lowest wear rates and highest hardness values were observed. The average coefficient of friction at room temperature was 0.1 and 0.3 at a speed of 21 m/s. The dominant wear mechanism at room temperature was abrasive wear as the wear rate increased linearly with an increase in load from 10 to 20 N. The scan speed had the most significant influence on the wear behaviour of the as-built high-entropy alloy attributed to the rapid rate of solidification which occurs at higher scan speeds.

Conclusions: The study examines the wear characteristics of high-entropy alloys fabricated via laser deposition technique in comparison with those fabricated via conventional routes. Although there were similarities in the phase structures of both techniques, the results showed that the wear resistance of the laser-deposited high-entropy alloy was comparatively higher than the same alloy prepared via conventional methods. Laser additive manufacturing was concluded to be a more successful method in fabricating high-entropy alloys.

Keywords: Tribology, High-entropy alloys, Laser metal deposition, Wear mechanism, COMSOL multiphysics

1 Background

Wear and friction are major engineering problems classified as the responses to a tribo-system because they describe the state of the two bodies in contact in the system [1]. Nonetheless, it is important to control the wear of materials to reduce maintenance costs and

*Correspondence: dadadupeola@gmail.com

[1] Chemical, Metallurgical and Materials Engineering, Tshwane University of Technology, Pretoria 0183, South Africa
Full list of author information is available at the end of the article

prevent the failure of the material during service for aero-engine applications [2]. To achieve this, wear-resistant materials must be developed for long life and stable operations. Several materials have been used and failed until recent years, with the emergence of high-entropy alloys and their characteristic features attracting research interest because of their high-entropy mixing and lattice distortion effect which gives the alloy strength preventing plastic deformation and dislocation movements [3–5]. Consequently, in the AlCoCrCuFeNi high-entropy alloy composition, there must be at least five elements between 5 and 35 at.% in near-equal or equimolar concentrations enabling the alloy to form structural stability and solid solution FCC, BCC or FCC + BCC structures attributed to the valence electron concentration (VEC) [6–8], small atomic radius difference δ and large enthalpy of mixing ΔH_{mix}, Ω [9, 10].

AlCoCrCuFeNi high-entropy alloys have distinctive microstructures and hydrophilic features, making them potential materials for anti-adherent applications [11]. However, with an average of about seven publications per year from 2016 to August 2021, the tribological properties reported in the literature are from high-entropy alloy systems fabricated via arc melting which has been reported to form defects that are detrimental to the mechanical properties of the alloy attributed to the slow solidification rate of the manufacturing process [12]. Hemphill et al. [13] recommended using advanced manufacturing methods in the synthesis of the high-entropy alloy as a solution to preventing the defects observed during the fabrication of as-cast $Al_{0.5}$CoCrCuFeNi high-entropy alloy responsible for the poor mechanical properties observed.

Yu et al. [14] examined the tribological behaviour of two high-entropy alloy systems ($AlCoCrFeNiTi_{0.5}$ and AlCoCrCuFeNi) prepared via arc melting under 90% hydrogen peroxide solution for propulsion applications because previous studies in the literature showed that the AlCoCrCuFeNi alloy system has good tribological properties in this solution [15]. The tests were carried out using a disc comprising stainless steel, SiC, and ZrO_2 ceramics as counterparts on a pin-on-disc tribo-tester at room temperature. The results showed that the wear mechanisms were delamination and adhesion, which led to a huge wear loss and a very high coefficient of friction when the high-entropy alloy was sliding against the ZrO_2 ceramic and stainless steel counter ball. However, the authors observed low wear loss and a coefficient of friction when the alloys were sliding against the SiC ceramic disc. Generally, the $AlCoCrFeNiTi_{0.5}$ had better wear properties than the AlCoCrCuFeNi high-entropy alloy under the SiC ceramic discs.

Luo et al. [16] tried improving the tribological properties of AlCoCrCuFeNi high-entropy alloy in 90% H_2O_2 solution by using heat treatment at various temperatures. However, the tests were performed using Si_3N_4. The results showed an increment in the wear loss from 3 to 11 μm and an improvement in the average coefficient of friction from 0.037 to 0.115 [17]. Prabu et al. [18] fabricated AlCoCrCuFeNi high-entropy alloy via laser surface alloying to improve the tribological properties of Ti–6Al–V alloy. The tests were carried out with varying loads of 35 N and 50 N on a pin-on-disc tribometer with a stainless steel disc as the counterpart material. The results showed that the high-entropy alloy showed both FCC and BCC phases with some intermetallic phases observed attributed to the titanium from the substrate which reacted with the high-entropy alloy during the laser alloying technique, which was also observed by other authors [19–21]. The laser-alloyed AlCoCrCuFeNi high entropy was 2.62 times more wear-resistant than the titanium alloy at a load of 50 N. For all loading conditions, the coefficients of friction of the high-entropy alloy and the titanium alloy increased. Nonetheless, the substrate had a higher coefficient of friction compared with the laser-alloyed high-entropy alloy with adhesive, abrasive, and severe plastic deformation observed as the wear mechanism for the titanium alloy, and mild abrasive wear mechanism was observed for the laser-alloyed AlCoCrCuFeNi high-entropy alloy.

Meng et al. [22] fabricated AlCoCrCuFeNi high-entropy alloy via laser melt injection on a magnesium substrate. The microstructural morphologies and tribological properties were investigated. The wear characteristics of the alloy were investigated using a universal wear machine at room temperature using alumina as the counterpart material. The results showed that the alloy had both FCC and BCC phases. The authors observed very low wear resistance attributed to the $CuMg_2$ phase, showing that the copper rejection negatively influences the wear properties of the alloy composition attributed to the brittle phase. In another study, the authors reinforced the high-entropy alloy with an A91D metal matrix composite [23]. The alloy was stable in the metal matrix composite attributed to the mixing enthalpy, and the tribological properties were significantly improved. Dolique et al. [11] fabricated AlCoCrCuFeNi high-entropy alloy via magnetron sputtering and tested the alloy using the ball-on-disc, ball-on-block, or pin-on-disc technique [24, 25].

Few studies varied the load and temperature in their study of the tribological behaviour of high-entropy alloys [26–28], and some varied the distance and speed [29–31], while others investigated the influence of alloying elements on the tribological properties of the high-entropy alloys

[32–34] with substantially low reports in the literature on the tribological behaviour of high-entropy alloys fabricated via the laser metal deposition (LMD) technique. Nonetheless, arc melting does not have as many advantages as laser processing does. Some benefits of laser deposition over conventional methods include high solidification, cooling, and velocity of heating rate. Small heat-affected zones, minimal shape distortion, and prevention of compositional segregation through solute trapping [21, 35, 36]. Rapid solidification rates of the laser deposition process limit elemental diffusion and control nucleation and growth, thus improving the mechanical properties of high-entropy alloys. These characteristic features are attributed to the increment in the BCC phase structure during solidification [21, 37, 38]. Other works that have been done by other authors can be seen here [39–46]

In this study, AlCoCrCuFeNi high-entropy alloy was fabricated via laser metal deposition to determine the tribological behaviour of the as-built high-entropy alloy for aerospace applications. The research investigates the influence of the load variation, the effect of the laser processing parameters, and solidification rates on the as-built alloys at room temperature for improved tribological properties compared to conventional fabrication techniques. To understand the microscale mechanisms causing material loss at the contact interface, finite element analysis using COMSOL multiphysics was performed to model the contact stress simulation of the 100cr6 steel counter ball on the as-built high-entropy alloy surface.

2 Methods

2.1 Material

The commercially procured elemental blend of AlCoCrFeNiCu powder was prepared via proprietary solid-state alloying by F. J Brodmann & Co, L.L.C, USA. Table 1 shows the as-received high-entropy alloy composition.

2.2 Methods

2.2.1 The laser deposition process

Fabrication of the as-received powders was carried out using the LENS system with a working envelope of $900 \times 1500 \times 900$ mm, a positional accuracy of $\pm$ 0.25 mm, across the working envelope, and a linear resolution of $\pm$ 0.025 mm. The system comprises two powder feeders, which allow the powdered metal samples to be delivered to the melt pool created by a 500 W Nd: YAG laser cell. Four nozzles direct streams of metal powder feed into the high-power laser beam that heats the baseplate on a table to create a tiny weld pool for material build-up. Both the nozzle and the table can be moved in a synchronized way to define the next layer of the part for metal deposition [47–49]. LENS equipment with a spatial resolution feature deposits the high-entropy alloy powders between 30 and 1 cm at rates up to 200 cm^3/hr. The process is repeated until the total composition is built. The LENS laser cell is powered by a 4.4 kW Rofin Sinar DY 044 Nd: YAG laser. The laser beam was delivered to a six-axis articulated arm robot via a 400- or 600-micron step-index optical fibre. The robot was also integrated with a DPK 400 two-axis positioner that provides an additional two axes of rotation. The beam delivery option had a Precitec YW50, a high YAG Ask weld module with beam shape capabilities, while a scanner was used for surface hardening. The laser processing parameters are shown in Table 2.

2.2.2 Microstructural characterization

The crystal structure and phase composition of the alloys were measured using a PANalytical XPERT-PRO X-ray diffraction system using a radiated Cu-Kα and $\lambda = 1.54056$ Å, while the scanning electron microscope (SEM) characterization was performed using Joel-JSM-6010/LA Plus Microscope.

2.2.3 Microhardness characterization

The microhardness tests were conducted under a 200-g load using a Matsuzawa Seiki MMT-X series Vickers hardness tester at 10 s loading time conditions.

2.2.4 Wear characterization

After fabrication, the as-built samples were cut into different sections using Struers Labotom-5 cutting machine and the cross section of each sample was mounted using

Table 2 Laser processing parameters

Alloy composition	Sample	Laser power (W) (J/s)	Scan speed (mm/s)	Beam diameter (mm)
AlCoCrCuFeNi	A	1200	8	2
	B	1200	12	2
	C	1400	12	2
	D	1600	10	2
	E	1600	12	2

Table 1 Chemical composition of AlCoCrFeNiCu HEA powder in weight percentage

Element	Al (wt%)	Co (wt%)	Cr (wt%)	Fe (wt%)	Ni (wt%)	Cu (wt%)
AlCoCrFeNiCu	42.95	11.09	10.24	13.52	10.36	11.84

a phenolic black conductive resin in an AMP 50 automatic mounting press machine. The mounted samples were ground using SiC grinding papers (grit sizes of 80, 320, 1200 and 4000) and polished (Tripoli, intermediates and finishing rouges) on a Struers tetrapol-25 grinding and polishing machine. The surface of the ground samples was polished until a mirror finish was obtained using Diapro MD-Mol 3-µm diamond suspension and colloidal silica of 0.04 µm OP-S suspensions for 5 min. The ground and polished samples were etched using aqua regia reagent by immersing each sample into the etchant for about 15 s; afterwards, the metallographically prepared as-built samples were taken for surface roughness test using a digital profilometer (Taylor Hobson, England), and the results showed that Ra was at 0.50 µm. The wear behaviour of the as-built samples was tested using an Anton Paar TRB^3 pin-on-disc Tribometer under ambient temperature. The setup used a 100cr6 steel counter ball sliding against the high-entropy alloy samples in a circular motion under a varied load of 10 N and 20 N, at a radius of 0.39 mm and an acquisition rate of 80 Hz under dry conditions. The wear rates and friction coefficients were investigated, and each sample was tested three times, with the average wear rate value reported. The optical micrographs of the wear tracks were observed using an Olympus BX_{51} light optical microscope.

2.2.5 Counter ball rolling friction finite element

The movement of the counter ball on the as-built high-entropy alloy was considered where the ball was assumed to rotate around the radius (R), the z-axis, rotational velocity (ω), and translational velocity (V), respectively, as shown in Fig. 1, where ξ is the corresponding indentation and F_n is the contact load between the ball and the alloy. Another assumption is that the ball is in a steady state and that it rolls purely on the surface of the alloy with rotational and translational velocities kept constant, showing that $V = R\omega$. The computational analysis was executed to get the stress field on the as-built high-entropy alloy.

It is also assumed that the as-built AlCoCrCuFeNi high-entropy alloy behaviour with the ball is inelastic; therefore, the distribution of pressure at the interface contact will be asymmetric and this will be shown at M_r which is at the opposite end to the rotation direction as:

$$M_r = \iint_s \sigma_{yy} x \mathrm{d}S \tag{1}$$

where the contact area is S and the stress tensor component along the y-axis is σ_{yy}. Therefore, the equation gives the rolling friction in terms of the stress only where F_n is the total contact applied load, given as:

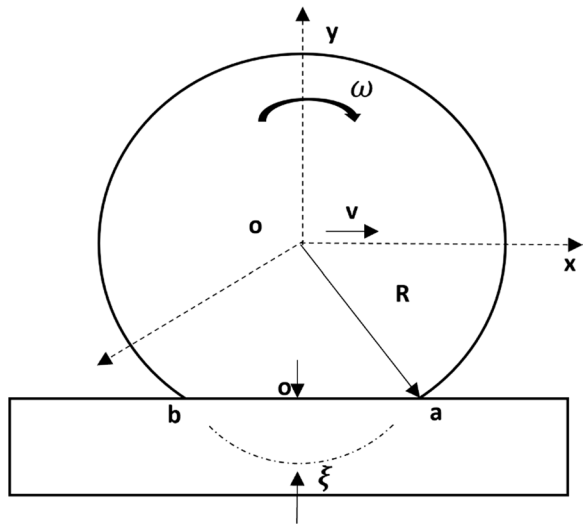

Fig. 1 Schematic diagram of the counter ball on the as-built AlCoCrCuFeNi high-entropy alloy

$$F_n = \iint_s \sigma_{yy} \mathrm{d}S \tag{2}$$

3 Results

3.1 Microstructure

The analysis of the X-ray diffraction patterns of AlCoCrCuFeNi HEA using an XPERT-PRO X-ray diffraction system is shown in Fig. 2. The analysis shows a solid solution of BCC and FCC structures due to the elemental composition of the AlCoCrCuFeNi HEA and its high-entropy effect [50].

The AlCoCrCuFeNi HEA shows a columnar dendritic structure shown in Fig. 3, and columnar dendritic structures are reported to have a strong preference for growing in one direction, which is almost at right angles with the interface attributed to the surface energy and the rate of solidification [51].

3.2 Microhardness

The laser power had the most significant influence on the hardness values of the alloys shown in Fig. 4.

3.3 Wear

An optical profilometry was used to calculate the wear volume at each laser parameter [52]. A TRB3 tribometer software version 8.1.8 calculated the wear rate in mm^3/Nm by dividing the wear volume by the sliding distance and normal load. From the result, it was observed that the wear rate decreases with an increase in the scanning speed at 12 mm/s as shown in Fig. 5.

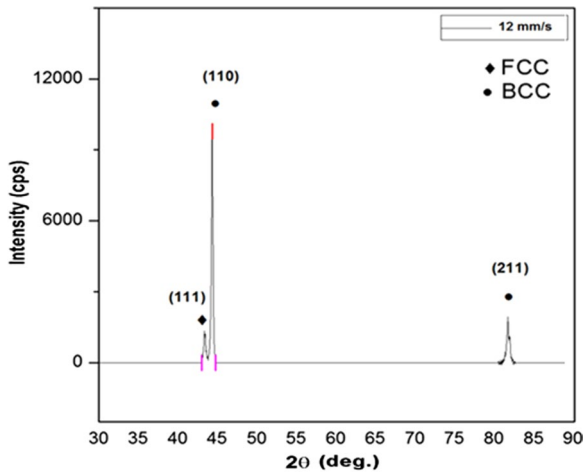

Fig. 2 XRD pattern of AlCoCrFeNiCu high-entropy alloy at 1600 W, 12 mm/s

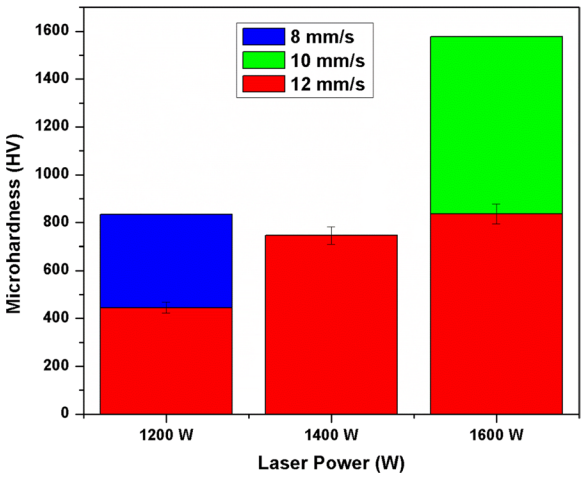

Fig. 4 Microhardness chart of AlCoCrCuFeNi HEA

3.3.1 Effect of the load variation on the wear characteristics of high-entropy alloys

The influence of the applied load variation on the wear volume of the as-built AlCoCrCuFeNi high-entropy alloy is shown in Fig. 6. The wear volume increases linearly as presented in Table 3 from 1.096E−06 mm^3 N m to 3.902E−04 mm^3 N m as the load increases from 10 to 20 N, respectively.

For both applied loads, the wear rates were in the order E > D > C > B > A. A comparative study of high-entropy alloys fabricated via casting and additive manufacturing is presented in Table 4.

The coefficient of friction for the AlCoCrCuFeNi high-entropy alloy is shown in Fig. 7a, b.

The optical morphology of the wear track of the as-built AlCoCrCuFeNi high-entropy alloy is shown in Fig. 8

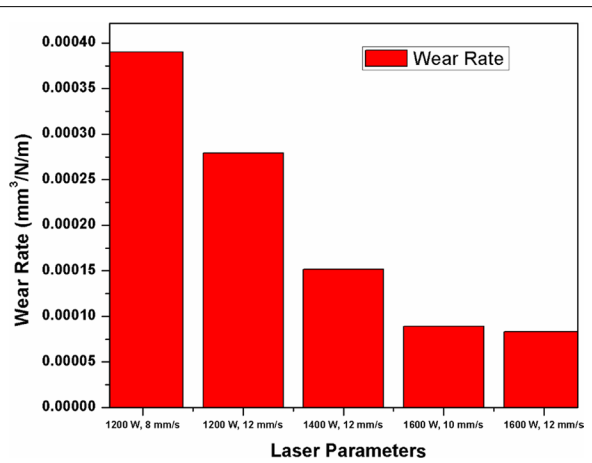

Fig. 5 Influence of laser parameters on the wear rate of AlCoCrFeNiCu high-entropy alloy at 20 N

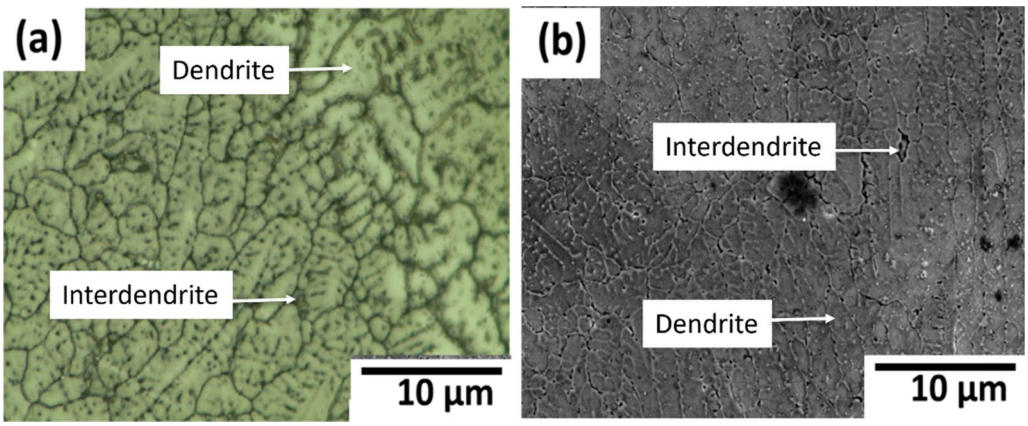

Fig. 3 **a** OPM images **b** SEM images of the microstructure of as-built AlCoCrFeNiCu high-entropy alloy at 1600 W, 12 mm/s

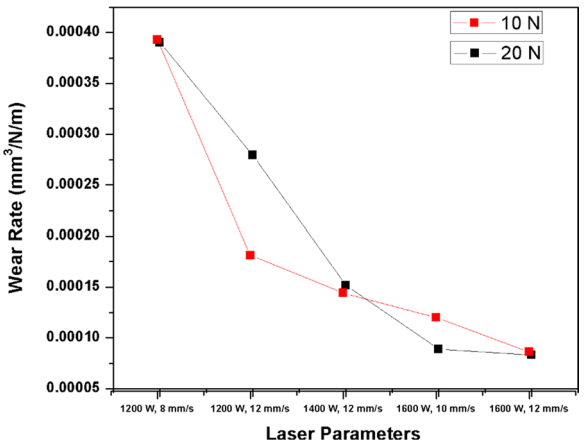

Fig. 6 Influence of load on the wear rate of AlCoCrCuFeNi high-entropy alloy at 10 N and 20 N

Table 3 Wear rates of AlCoCrFeNiCu HEA at 10 N and 20 N applied loads

Alloy composition	Sample	Wear rates (mm^3 N m) at 10 N applied load	Wear rates (mm^3 N m) at 20 N applied load
AlCoCrCuFeNi	A	2.97E−05	3.902E−04
	B	9.965E−06	2.794E−04
	C	6.511E−06	1.516E−04
	D	4.267E−06	8.893E−05
	E	1.096E−06	8.331E−05

3.4 Finite element simulation of the contact stress

Wear is a destructive mechanism that involves different microscale actions resulting in material loss at the interface of the contact between the ball and the alloy. An increase in the contact stresses leads to system failures. Hence, the contact stress significantly influences the wear mechanism of the alloying system. Therefore, COMSOL multiphysics was used to develop a model to investigate the von Mises stress which governs the initiation of plasticity in the HEA system at the interface of the 100cr6 steel counter ball. The as-built AlCoCrCuFeNi high-entropy alloy at 1600 W and 12 mm/s; sample E's properties are listed in Table 5 which were also related to the rolling friction analysis using the equation:

$$\mu_R = \frac{M_r}{F_n R} = f\left(\frac{F_n}{\mathrm{ER}^2}, \frac{\eta\omega}{E}, \nu\right) \tag{3}$$

The rolling friction coefficient is presented as μ_R, the Poisson's ratio is given as ν, the normalized velocity is symbolized as $\frac{\eta\omega}{E}$, the normalized contact load is denoted as $\frac{F_n}{\mathrm{ER}^2}$.

The finite element results of the contact stresses on the as-built high-entropy alloy is shown in Fig. 9. The 3D geometry of the simulation is shown in Fig. 9a, while Fig. 9b shows the 2D geometry set at a radius of 0.6 m, width of 2 m, and height of 0.2 m dimension of the strain energy density at (m/s^2). The mesh configuration is shown in Fig. 9c, while 2D representation of the von Mises stress is shown in Fig. 9d.

4 Discussion

4.1 Microstructure analysis

Despite the elemental effect of Co and Ni forming the FCC phase and Cu segregating to the interdendritic region to form a Cu-rich FCC phase attributed to its high positive enthalpy, the AlCoCrCuFeNi HEA was still more of a BCC solid solution structure with its highest peak at 45° attributed to the large volume fraction of Al in the composition and its large atomic radius which is also known to form the BCC structure compared with other principal elements in the composition [54, 55].

The BCC structure has a lower atomic packing density than the FCC, resulting in the accommodation of larger solute atoms like Al [14]. Suggesting that constituent elements significantly influence the phase formation of the as-built AlCoCrCuFeNi high-entropy alloy. The calculated parameters shown in Table 6 for the prepared as-built alloy suggest that the alloy meets the criterion for the formation of solid solution structures since $\Omega > 1$, according to Kumar et al. [56].

Dendrites and interdendritic structures were observed, and the interdendritic region from EDS analysis showed that it consists mostly of Cu attributed to the low binding

Table 4 Manufacturing technique comparative study of tribological properties of high-entropy alloys

Alloy composition	Fabrication technique	Testing method	Load (*N*)	Speed or frequency	Wear rate (mm^3/Nm)	Friction	References
AlCoCrFeNi	Casting	Pin-on-disc	15	100 mm/s	–	0.74	[53]
$Al_{0.5}CoCrFeNiTi_{0.5}$	Casting	Ball-on-disc	10	–	–	0.35	[54]
$Al_{0.5}CoCrCuFeNi$	Casting	Pin-on-disc	29.4	0.5 m/s	0.00070000	0.5	[6]
$Al_1CoCrCuFeNi$	Casting	Pin-on-disc	29.4	0.5 m/s	0.00050000	0.48	[6]
AlCoCrCuFeNi	Additive manufacturing	Pin-on-disc	10 and 20	21 m/s	0.00008331, 0.000001096	0.1, 0.3	This study

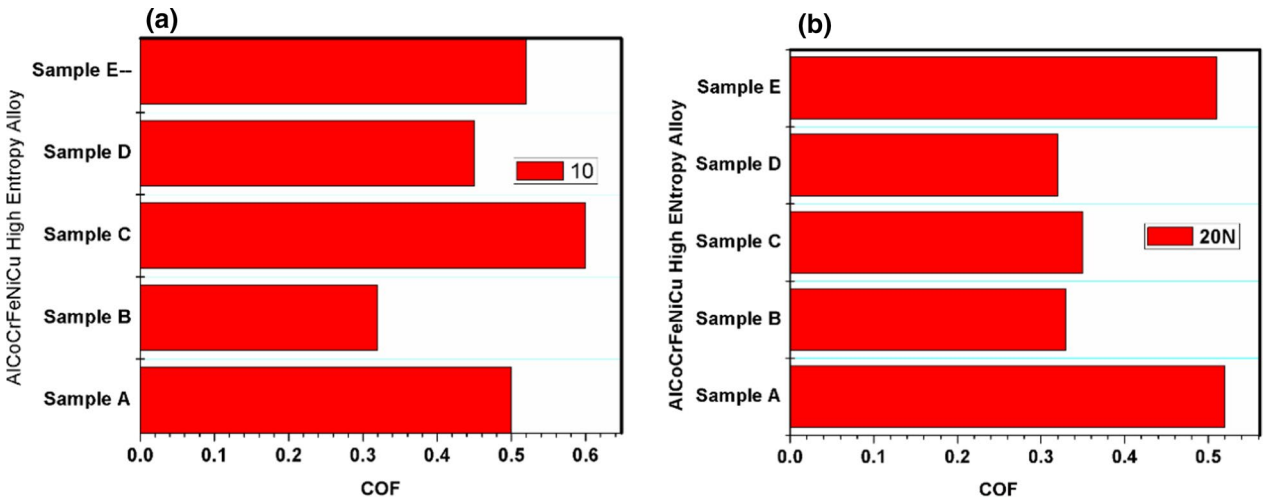

Fig. 7 Coefficient of friction for AlCoCrCuFeNi high-entropy alloy at **a** 10 N **b** 20 N

energy of Cu with other elements like Co, Fe, Ni, and C [57]. Hence, suggesting that the segregation of elements in as-built HEAs is significantly influenced by the miscibility between the alloying elements and the mixing enthalpy.

4.2 Microhardness analysis

There was an increase in the hardness values from 389 to 837 HV as the laser power increased from 1200 to 1600 W attributed to the increase in dilution rates with the increase in laser power resulting in increased hardness [58]. Consequently, Sample E with laser power of 1600 W had the highest hardness value at 837 HV, while sample A with laser power of 1200 W had the lowest hardness value of 445 HV. The increase in the hardness properties of the amalgams can also be attributed to the strengthening mechanism due to the significant BCC phases observed. The BCC phase is stronger than the FCC phase because, in the packing planes of the BCC {110}, a slip along this plane is more difficult than the FCC {111} plane resulting in higher lattice friction for dislocation motion and lower interplanar spacing which accounts for the solution hardening mechanism [59].

4.3 Wear analysis

The wear results show that the scan speed had a significant influence on the tribological properties of the alloy, which is largely attributed to the rate of solidification of the laser deposition process. At a high speed, the rate of solidification increases, resulting in grain refinement, thus increasing the strength of the alloy, which contributes to the alloy's ability to resist material loss [60]. The high aluminium content in the composition also stabilizes the solid solution BCC structure, which is also responsible for the strengthening mechanism of the alloy, resisting plastic deformation by abrasive wear and improving the wear resistance [61, 62]. The lowest wear rates were observed with sample *E* at a high laser power of 1600 W, correlating with the hardness values of the alloy. Consequently, the higher the hardness values, the better the wear resistance. The as-built AlCoCrCuFeNi high-entropy alloy of this study shows better wear resistance than alloys fabricated via conventional techniques suggesting that the laser deposition method has a clear advantage over conventional techniques, thus, positively influencing the wear resistance of high-entropy alloys which will be useful for applications where wear is a major factor.

The results of the coefficient of friction were achieved at a variation of 10 N and 20 N, respectively, under dry sliding conditions. The lowest average coefficient of friction values of 0.1 were observed at 1600 W and 12 mm/s at a load of 10 N and 0.075 at a load of 20 N. At 10 N, the COF sharply increases until it reaches a steady state before decreasing slightly. The reduction in friction may be attributed to the surface of the alloy at 1400 W and 12 mm/s developing a thin surface layer during sliding which is transferred to the surface of the counterpart via adhesion causing displacements at the interface between the transferred layer and the surface of the high-entropy alloy.

Generally, the COF varied from 0.3 to 0.5 as the laser scan speed reduced [1, 63]. It was observed that the best resistance was at a reduced coefficient of friction and at a high scan speed of 12 mm/s attributed to the solid solution strengthening effect of the BCC

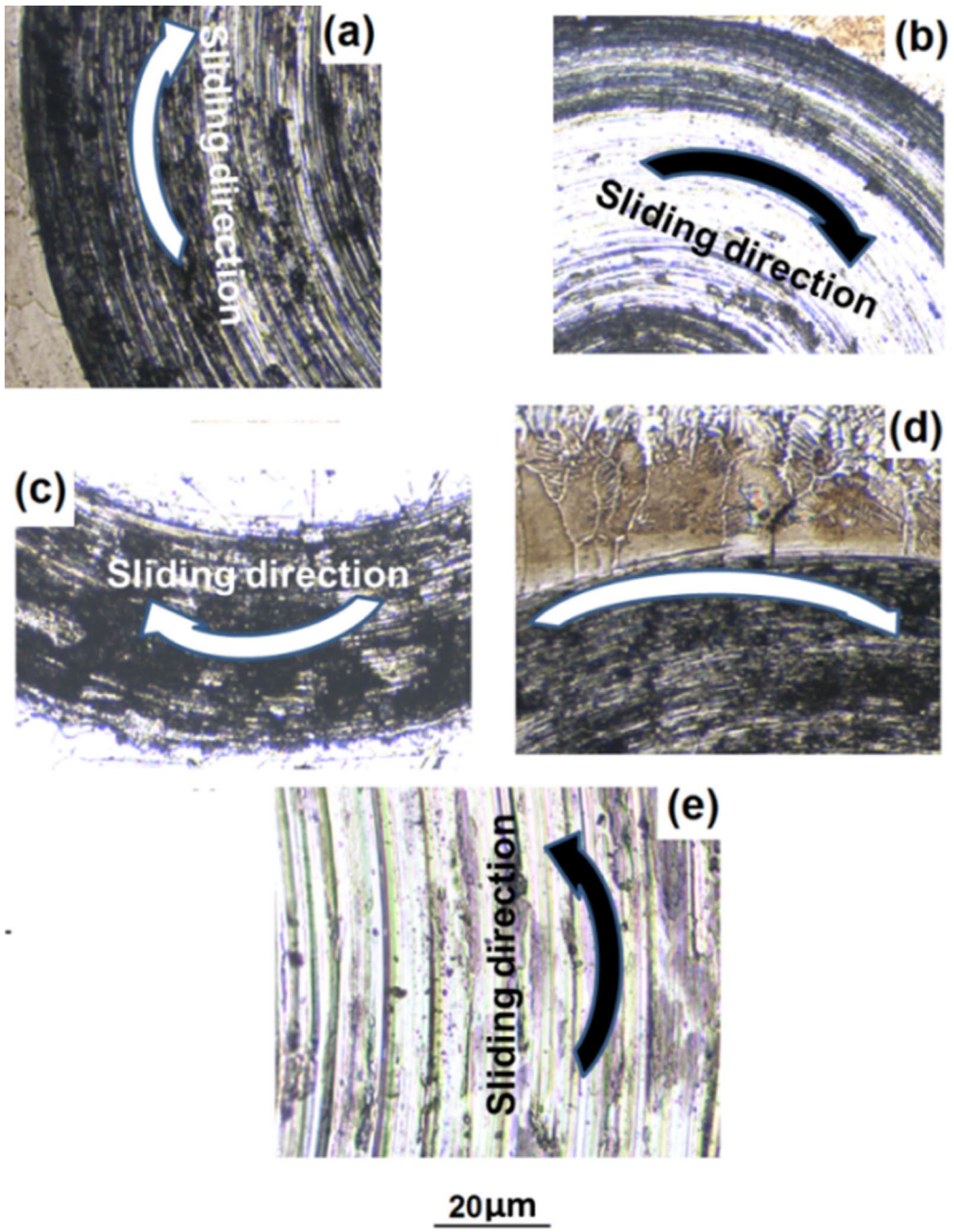

Fig. 8 Worn surface morphology of sample **a**–**e** at a load of 20 N under different processing parameters

phase at a rapid solidification rate when the scan speed is high, which produces reduced grain size. According to Hall–Petch relations, the as-built alloy has a higher resistance to deformation due to the small grain size, resulting in dislocation and grain boundary strengthening, thus, preventing the surface of the alloys from wear [64–66]. This shows that the laser processing parameter has a significant influence on the wear

Table 5 Parameters used for the simulation

Variable	Symbol	Value
Young modulus	GPa	149
Density	g/cm^3	7.240
Radius of sphere	*R*	0.6 m
Poisson's ratio	*v*	0.3
Yield strength	GPa	1.47

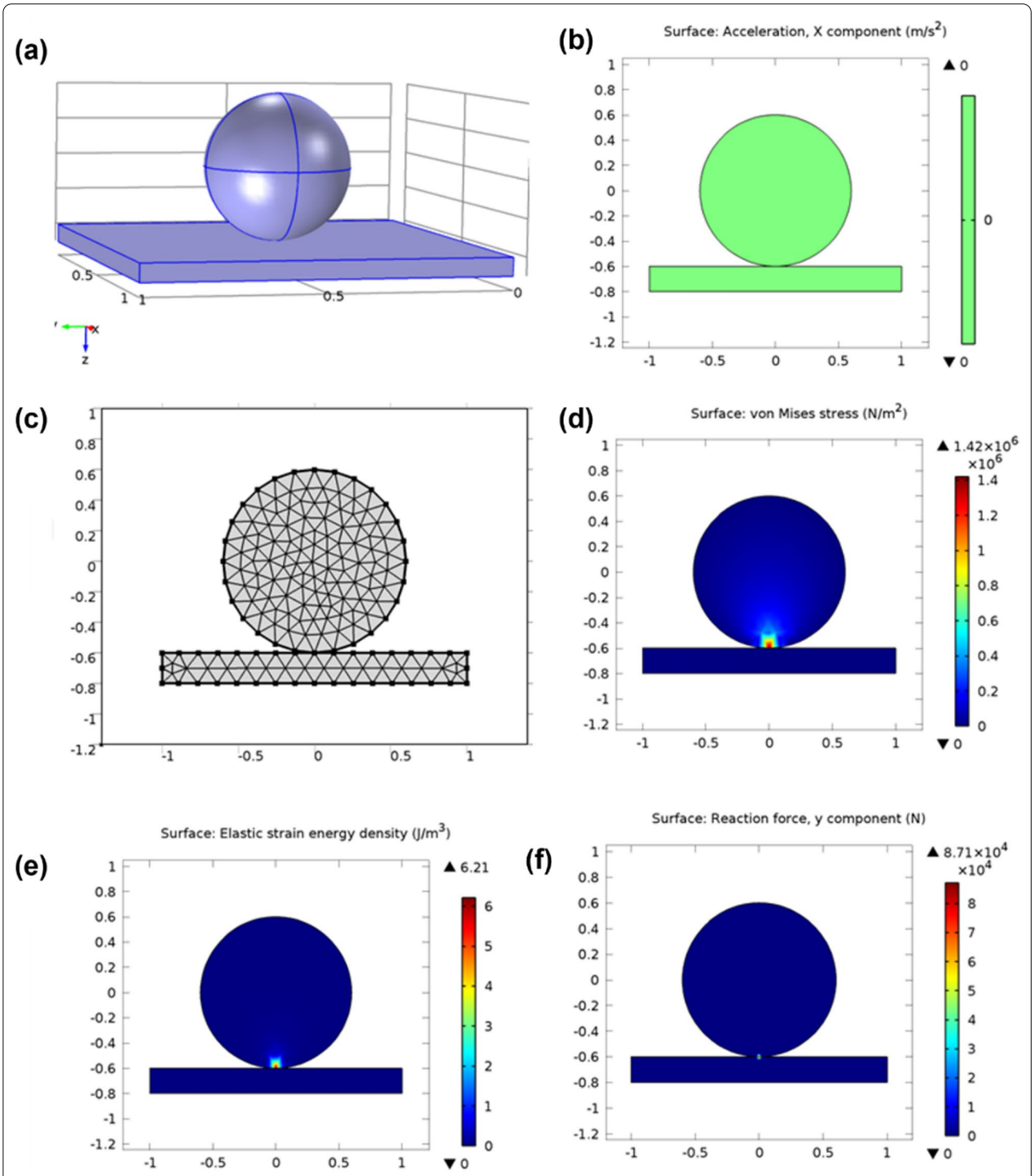

Fig. 9 Results of the COMSOL multiphysics counter ball rolling friction analysis **a** 3D geometry **b** 2D geometry showing the energy density **c** the mesh **d** the 2D plot of the von Mises stress variation at a contact point between the stationary 100Cr6 ball and the rotating as-built AlCoCrCuFeNi HEA **e** the 2D plot of the velocity and the elastic strain energy **f** 2D plot of the reaction force of the y component

Table 6 Calculated parameters for the design of AlCoCrCuFeNi HEAs [45]

High-entropy alloy composition	δ	ΔH_{mix} (kJ/mol)	S_c (ke per atom)	ϕ	ΔS_{mix} (kJ/mol)	VEC	ΔG (J/mol)	Δ_x	Ω	ΔS_σ/k
AlCoCrFeNiCu	5.28	− 4.78	1.79	14.12	14.89	7.83	− 4780	0.119	5.0	0.046

behaviour of the as-built high-entropy alloys. The wear resistance increases with the load because more debris is generated at a higher load, which adheres to the surface of the alloy, reducing the contact between the wear medium and the surface of the alloy [67, 68]. Another contribution to the wear resistance of the alloy is the formation of oxide films on the surface of the as-built alloy [69]. The rise in temperature during wear attributed to the friction heat accumulated forms oxide films when oxygen is in contact with the alloying elements at higher load results in a lower wear rate. At 20 N, where the lowest wear rates were observed. Compared with other samples, E and B had fewer worn surfaces attributed to having the best wear resistance and highest hardness of 837 HV and 700 HV, respectively, from previous studies [70]. Wear particles and grooves were observed parallel to the sliding direction, and the wear mechanism was abrasive wear.

4.4 Finite element analysis

The finite element analysis was developed with the solid mechanics interface in a stationary study for stress modelling, established on the standards of momentum balance equations. An assumption that the strains and displacements remained small led to the following governing equations:

$$-\nabla \cdot \sigma = F_v, \sigma = s \tag{4}$$

$$s = S_0 = C : (\in - \in_0 - \in_{\text{inel}}) \tag{5}$$

$$\in = \frac{1}{2}\left[(\nabla_u)^T + \nabla_u\right] \tag{6}$$

where F_v is the body force,u is the displacement, σ s the stress tensor, and $\in$ is the strain tensor. No other forces were considered during simulation asides the pressure exerted on the surface of the alloy by the counter ball.

The centre of the counter interface shows the highest stress levels, which is inevitably responsible for the generation of asperity. Increasing the contact stresses will cause severe deformation to occur. Once the yield stress provided in Table 6 is greater than the von Mises stress, leading less asperity. This computational result corroborates with the experimental results and the images of the worn surfaces of Sample E, which show predominant elastic deformation.

5 Conclusion

In this study, AlCoCrCuFeNi high-entropy alloys at different processing parameters were fabricated using laser metal deposition. The influence of the laser parameters and load variations on the hardness and wear properties of the as-built alloy were investigated in dry conditions because the study of the mechanical properties of high-entropy alloys is essential for designing components for aerospace applications. The crystal morphology showed the alloy has solid solution phases, BCC + FCC structures with a predominant BCC phase and columnar dendritic microstructures. The laser power had the most significant influence on the hardness values of the alloys. Sample E fabricated with laser power of 1600 W and scanning speed of 12 mm/s had 88% higher hardness values than Sample A fabricated with laser power of 1200 W and scanning speed of 8 mm/s. This is attributed to the rate of solidification of the laser deposition process at a high laser power and scan speed. The average coefficient of friction at room temperature was the lowest (0.1 and 0.3) at a speed of 21 m/s an acquisition rate of 80 Hz attributed to the properties of individual elements in the alloying composition and their respective processing parameters. The wear rate of the as-built alloy was at the lowest at the highest scan speed of 12 mm/s and laser power of 1600 W attributed to the rapid rate of solidification of the laser deposition process at an increased scan speed and the laser power. The finite element results showed that the deformation was predominantly elastic. Compared to conventional methods, laser-deposited AlCoCrCuFeNi high-entropy alloys showed better wear resistance as materials for aerospace structural applications.

Abbreviations

HEAs: High-entropy alloys; HEA: High-entropy alloy; FCC: Face-centred cubic; BCC: Body-centred cubic; VEC: Valence electron concentration; LMD: Laser metal deposition; SEM: Scanning electron microscope.

Acknowledgements

The authors appreciate Prof. S. Pityana at the Laser Enabled Manufacturing Resource Group at the Council for Scientific and Industrial Research CSIR, and the Surface Engineering Research Laboratory (SERL) for their Technical Support.

Author contributions
MD involved in conceptualization, data curation, and editing and reviewing of draft. PP involved in conceptualization, supervision, data curation, and editing and reviewing of draft. NM involved in supervision and editing and reviewing of drafts. SA involved in conceptualization, supervision, article draft review, and revision. All authors read and approved the final manuscript.

Funding
Not applicable.

Availability of data and materials
Not applicable.

Declarations

Ethics approval and consent to participate
Not applicable.

Consent for publication
Not applicable.

Competing interests
All authors declare that they have no competing interests.

Author details
[1]Chemical, Metallurgical and Materials Engineering, Tshwane University of Technology, Pretoria 0183, South Africa. [2]Council for Scientific and Industrial Research, Pretoria 0184, South Africa. [3]Metallurgical and Materials Engineering, University of Lagos, Akoka 100213, Nigeria. [4]Department of Industrial Engineering, Durban University of Technology, Durban, South Africa.

Received: 5 August 2022 Accepted: 22 September 2022
Published online: 08 November 2022

References

1. Abdulrahman KO, Mahamood RM, Akinlabi ET, Adediran AA (2021) Effect of laser power on the microstructure and mechanical properties of laser deposited titanium aluminide composite. Adv Mater Process Technol 25(3):1–12
2. Akgül A, Hashemi M, Inc M, Raheem S (2017) Constructing two powerful methods to solve the Thomas–Fermi equation. Nonlinear Dyn 87:1435–1444
3. Akgül A, Inc M, Kilicman A, Baleanu D (2016) A new approach for one-dimensional sine-Gordon equation. Adv Differ Equ 2016:1–20
4. Beaman JJ, Barlow JW, Bourell DL, Crawford RH, Marcus HL, Mcalea KP (1997) Solid freeform fabrication: a new direction in manufacturing, vol 2061. Kluwer Academic Publishers, Norwell, pp 25–49
5. Boudjema I, Djilali S (2018) Turing-Hopf bifurcation in Gauss-type model with cross diffusion and its application. Nonlinear Stud 25:3
6. Boutarfa B, Akgül A, Inc M (2017) New approach for the Fornberg–Whitham type equations. J Comput Appl Math 312:13–26
7. Cagirici M, Wang P, Ng FL, Nai MLS, Ding J, Wei J (2021) Additive manufacturing of high-entropy alloys by thermophysical calculations and in situ alloying. J Mater Sci Technol 94:53–66
8. Cai Z, Cui X, Liu Z, Li Y, Dong M, Jin G (2018) Microstructure and wear resistance of laser cladded Ni–Cr–Co–Ti–V high-entropy alloy coating after laser remelting processing. Opt Laser Technol 99:276–281
9. Cai Z, Jin G, Cui X, Liu Z, Zheng W, Li Y, Wang L (2016) Synthesis and microstructure characterization of Ni–Cr–Co–Ti–V–Al high entropy alloy coating on Ti–6Al–4V substrate by laser surface alloying. Mater Charact 120:229–233
10. Cai Z, Wang Z, Hong Y, Lu B, Liu J, Li Y, Pu J (2021) Improved tribological behavior of plasma-nitrided AlCrTiV and AlCrTiVSi high-entropy alloy films. Tribol Int 163:107195
11. Chen M, Shi XH, Yang H, Liaw PK, Gao MC, Hawk JA, Qiao J (2018) Wear behavior of $Al_{0.6}$CoCrFeNi high-entropy alloys: effect of environments. J Mater Res 33:3310–3320
12. Chen S, Aitken ZH, Wu Z, Yu Z, Banerjee R, Zhang Y-W (2020) Hall–Petch and inverse Hall–Petch relations in high-entropy CoNiFeAl_xCu_{1-x} alloys. Mater Sci Eng A 773:138873
13. Dąbrowa J, Cieślak G, Stygar M, Mroczka K, Berent K, Kulik T, Danielewski M (2017) Influence of Cu content on high temperature oxidation behavior of AlCoCrCu_xFeNi high entropy alloys ($x = 0$; 0.5; 1). Intermetallics 84:52–61
14. Dada M, Popoola P, Mathe N, Pityana S, Adeosun S, Aramide O, Lengopeng T (2020) Process optimization of high entropy alloys by laser additive manufacturing. Eng Rep 2:e12252
15. Diao H, Feng R, Dahmen KA, Liaw P (2017) Fundamental deformation behavior in high-entropy alloys: an overview. Curr Opin Solid State Mater Sci 21:252–266
16. Djilali S, Benahmadi L, Tridane A, Niri K (2020) Modeling the impact of unreported cases of the COVID-19 in the North African countries. Biology 9:373
17. Djilali S, Bentout S (2021) Global dynamics of SVIR epidemic model with distributed delay and imperfect vaccine. Results Phys 25:104245
18. Dolique V, Thomann A-L, Brault P, Tessier Y, Gillon P (2009) Complex structure/composition relationship in thin films of AlCoCrCuFeNi high entropy alloy. Mater Chem Phys 117:142–147
19. Duan H, Wu Y, Hua M, Yuan C, Wang D, Tu J, Kou H, Li J (2013) Tribological properties of AlCoCrFeNiCu high-entropy alloy in hydrogen peroxide solution and in oil lubricant. Wear 297:1045–1051
20. Duchaniya RK, Pandel U, Rao P (2021) Coatings based on high entropy alloys: an overview. Mater Today Proc 44:4467–4473
21. Erdoğan A, Gök MS, Zeytin S (2020) Analysis of the high-temperature dry sliding behavior of CoCrFeNi$Ti_{0.5}Al_x$ high-entropy alloys. Friction 8:198–207
22. Ezugwu E (2005) Key improvements in the machining of difficult-to-cut aerospace superalloys. Int J Mach Tools Manuf 45:1353–1367
23. Geng Y, Tan H, Wang L, Tieu AK, Chen J, Cheng J, Yang J (2021) Nano-coupled heterostructure induced excellent mechanical and tribological properties in AlCoCrFeNi high entropy alloy. Tribol Int 154:106662
24. Goddard J, Wilman H (1962) A theory of friction and wear during the abrasion of metals. Wear 5:114–135
25. Gu Z, Xi S, Sun C (2020) Microstructure and properties of laser cladding and $CoCr_{2.5}FeNi_2Ti_x$ high-entropy alloy composite coatings. J Alloys Compd 819:152986
26. Guo S (2015) Phase selection rules for cast high entropy alloys: an overview. Mater Sci Technol 31:1223–1230
27. Hemphill MA, Yuan T, Wang G, Yeh J, Tsai C, Chuang A, Liaw P (2012) Fatigue behavior of $Al_{0.5}$CoCrCuFeNi high entropy alloys. Acta Mater 60:5723–5734
28. Joseph J, Haghdadi N, Annasamy M, Kada S, Hodgson P, Barnett M, Fabijanic D (2020) On the enhanced wear resistance of CoCrFeMnNi high entropy alloy at intermediate temperature. Scr Mater 186:230–235
29. Joseph J, Haghdadi N, Shamlaye K, Hodgson P, Barnett M, Fabijanic D (2019) The sliding wear behaviour of CoCrFeMnNi and AlxCoCrFeNi high entropy alloys at elevated temperatures. Wear 428:32–44
30. Kasar AK, Scalaro K, Menezes PL (2021) Tribological properties of high-entropy alloys under dry conditions for a wide temperature range—a review. Materials 14:5814
31. Kato K (2000) Wear in relation to friction—a review. Wear 241:151–157
32. Kozak R, Sologubenko A, Steurer W (2015) Single-phase high-entropy alloys—an overview. Zeitschrift für Kristallographie-Cryst Mater 230:55–68
33. Kucza W, Dąbrowa J, Cieślak G, Berent K, Kulik T, Danielewski M (2018) Studies of "sluggish diffusion" effect in Co–Cr–Fe–Mn–Ni, Co–Cr–Fe–Ni and Co–Fe–Mn–Ni high entropy alloys; determination of tracer diffusivities by combinatorial approach. J Alloys Compd 731:920–928
34. Kumar A, Dhekne P, Swarnakar AK, Chopkar MK (2017) Analysis of Si addition on phase formation in AlCoCrCuFeNiSi_x high entropy alloys. Mater Lett 188:73–76
35. Li W, Liu P, Liaw PK (2018) Microstructures and properties of high-entropy alloy films and coatings: a review. Mater Res Lett 6:199–229
36. Liang CJ, Wang CL, Liang ML, Xie YG, Liu WJ, Yang JJ, Li X, Liu C, Zhou SF (2022) Effect of different durations on the microstructure and tribological behavior of $(Co_{1.5}FeNi)\ 90Ti_6Al_4$ high entropy alloy. Vacuum 195:110677

37. Lin D-Y, Zhang N-N, He B, Zhang G-W, Zhang Y, Li D-Y (2017) Tribological properties of $FeCoCrNiAlB_x$ high-entropy alloys coating prepared by laser cladding. J Iron Steel Res Int 24:184–189
38. Liu X, Liu X, Altounian Z, Tu G (2006) Microstructures of $(Fe_{0.88}Co_{0.12})_{82}La_7Si_{11}$ prepared by arc-melting/melt spinning and subsequent annealing. Appl Phys A 82:339–343
39. Liu Y, Xie Y, Cui S, Yi Y, Xing X, Wang X, Li W (2021) Effect of Mo element on the mechanical properties and tribological responses of $CoCrFeNiMo_x$ high-entropy alloys. Metals 11:486
40. Lu Y, Jiang H, Guo S, Wang T, Cao Z, Li T (2017) A new strategy to design eutectic high-entropy alloys using mixing enthalpy. Intermetallics 91:124–128
41. Luo X, Li J, Jin Y, Hu C, Jia D, Zhan S, Yu Y, Hua M, Duan H (2020) Heat treatment influence on tribological properties of AlCoCrCuFeNi high-entropy alloy in hydrogen peroxide-solution. Metals Mater Int 26:1286–1294
42. Malatji N, Popoola A, Lengopeng T, Pityana S (2020) Tribological and corrosion properties of laser additive manufactured AlCrFeNiCu high entropy alloy. Mater Today Proc 28:944–948
43. Mary SJ, Nagalakshmi R, Epshiba R (2015) High entropy alloys properties and its applications—an overview. Eur Chem Bull 4:279–284
44. Meng G, Lin X, Xie H, Yue TM, Ding X, Sun L, Qi M (2016) The effect of Cu rejection in laser forming of AlCoCrCuFeNi/Mg composite coating. Mater Des 108:157–167
45. Meng G, Yue TM, Lin X, Yang H, Xie H, Ding X (2015) Laser surface forming of AlCoCrCuFeNi particle reinforced AZ91D matrix composites. Opt Laser Technol 70:119–127
46. Modanli M, Akgül A (2017) Numerical solution of fractional telegraph differential equations by theta-method. Eur Phys J Spec Top 226:3693–3703
47. Ocelík V, Janssen N, Smith S, De Hosson JTM (2016) Additive manufacturing of high-entropy alloys by laser processing. JOM 68:1810–1818
48. Page T, Knight J (1989) Factors affecting the tribological behaviour of thin hard TiN and TiC coatings. Surf Coat Technol 39:339–354
49. Poulia A, Georgatis E, Karantzalis A (2019) Evaluation of the microstructural aspects, mechanical properties and dry sliding wear response of MoTaNbVTi refractory high entropy alloy. Met Mater Int 25:1529–1540
50. Prabu G, Duraiselvam M, Jeyaprakash N, Yang C-H (2021) Microstructural evolution and wear behavior of AlCoCrCuFeNi high entropy alloy on Ti–6Al–4V through laser surface alloying. Met Mater Int 27:2328–2340
51. Shuai C, Yang Y, Wu P, Lin X, Liu Y, Zhou Y, Feng P, Liu X, Peng S (2017) Laser rapid solidification improves corrosion behavior of Mg–Zn–Zr alloy. J Alloys Compd 691:961–969
52. Souna F, Djilali S, Charif F (2020) Mathematical analysis of a diffusive predator-prey model with herd behavior and prey escaping. Math Model Nat Phenom 15:23
53. Tsai M-H (2013) Physical properties of high entropy alloys. Entropy 15:5338–5345
54. Tsai M-H, Yeh J-W (2014) High-entropy alloys: a critical review. Mater Res Lett 2:107–123
55. Tung C-C, Yeh J-W, Shun T-T, Chen S-K, Huang Y-S, Chen H-C (2007) On the elemental effect of AlCoCrCuFeNi high-entropy alloy system. Mater Lett 61:1–5
56. Verma A, Tarate P, Abhyankar A, Mohape M, Gowtam D, Deshmukh V, Shanmugasundaram T (2019) High temperature wear in $CoCrFeNiCu_x$ high entropy alloys: the role of Cu. Scr Mater 161:28–31
57. Wang W-R, Wang W-L, Wang S-C, Tsai Y-C, Lai C-H, Yeh J-W (2012) Effects of Al addition on the microstructure and mechanical property of $Al_xCoCrFeNi$ high-entropy alloys. Intermetallics 26:44–51
58. Wu J-M, Lin S-J, Yeh J-W, Chen S-K, Huang Y-S, Chen H-C (2006) Adhesive wear behavior of $Al_xCoCrCuFeNi$ high-entropy alloys as a function of aluminum content. Wear 261:513–519
59. Yadaw RC, Singh SK, Chattopadhyaya S, Kumar S, Singh R (2018) Tribological behavior of thin film coating—a review. Int J Eng Technol 7:1656–1663
60. Yang X, Zhang J, Sagar S, Dube T, Kim B-G, Jung Y-G, Koo DD, Jones A, Zhang J (2021) Molecular dynamics modeling of mechanical and tribological properties of additively manufactured AlCoCrFe high entropy alloy coating on aluminum substrate. Mater Chem Phys 263:124341
61. Yeh J-W (2016) Overview of high-entropy alloys. High-entropy alloys. Springer
62. Yu Y, He F, Qiao Z, Wang Z, Liu W, Yang J (2019) Effects of temperature and microstructure on the triblogical properties of $CoCrFeNiNb_x$ eutectic high entropy alloys. J Alloys Compd 775:1376–1385
63. Yu Y, Wang J, Li J, Kou H, Duan H, Li J, Liu W (2015) Tribological behavior of AlCoCrCuFeNi and $AlCoCrFeNiTi_{0.5}$ high entropy alloys under hydrogen peroxide solution against different counterparts. Tribol Int 92:203–210
64. Yu Y, Wang J, Li J, Kou H, Liu W (2015) Characterization of BCC phases in $AlCoCrFeNiTi_x$ high entropy alloys. Mater Lett 138:78–80
65. Yu Y, Wang J, Yang J, Qiao Z, Duan H, Li J, Li J, Liu W (2019) Corrosive and tribological behaviors of AlCoCrFeNi-M high entropy alloys under 90 wt.% H_2O_2 solution. Tribol Int 131:24–32
66. Yu Y, Zhang B, Zhu S, Zhang Z, Lu W, Shen T, Wang Z (2020) Microstructural and tribological characteristics of in situ induced chrome carbide strengthened CoCrFeMnNi high-entropy alloys. J Mater Eng Perform 29:3714–3722
67. Zabinski J, Corneille J, Prasad S, Devitt MCN, Bultman J (1997) Lubricious zinc oxide films: synthesis, characterization and tribological behaviour. J Mater Sci 32:5313–5319
68. Zhang T, Liu H, Hao J, Chen P, Yang H (2021) Evaluation of microhardness, tribological properties, and corrosion resistance of CrFeNiNbTi high-entropy alloy coating deposited by laser cladding. J Mater Eng Perform 12:1–11
69. Zhang Y, Han T-F, Xiao M, Shen Y-F (2020) Effect of process parameters on the microstructure and properties of laser-clad $FeNiCoCrTi_{0.5}$ high-entropy alloy coating. Int J Miner Metall Mater 27:630
70. Zheng B, Liu QB, Zhang LY (2013) Microstructure and properties of MoFeCrTiW high-entropy alloy coating prepared by laser cladding. Adv Mater Res 83:63–66

Publisher's Note